Solid-state nuclear magnetic resonance as a tool for investigating the halogen bond

UNIVERSITÀ DEGLI STUDI DI TORINO

Solid-state nuclear magnetic resonance as a tool for investigating the halogen bond

Received 00th January 20xx,
Accepted 00th January 20xx

DOI: 10.1039/x0xx00000x

P. Cerreia Vioglio, M. R. Chierotti and R. Gobetto*

We provide a review of the state-of-the-art of solid-state nuclear magnetic resonance (SSNMR) spectroscopy applied to the study of the halogen bond interaction. The SSNMR approach yields a wealth of information complementary or alternative to X-ray crystallography, thus providing similar, yet different insight into the halogen bond. Indeed, SSNMR parameters can be used to probe powders at both molecular and crystal structure level, without needing highly crystalline samples or special preparations. This Highlight article serves as a tutorial example of the SSNMR strategies to characterize the halogen bond, and is based on a comprehensive literature survey and the discussion of relevant NMR parameters. Unresolved problems and future directions in the field are also summarized.

1. Introduction

The halogen bond (XB) is a non-covalent interaction with unique physicochemical properties, such as directionality, strength tunability, hydrophobicity and selectivity.[1] Although the existence of an interaction between halogen atoms and Lewis bases has been known from XIX century,[2] its potential has been recognized only during the last twenty years.[3–8] XB has today become a routinely used tool in modern supramolecular chemistry, influencing advances in chemistry,[9,10] materials science,[11,12] and biochemistry.[13,14] The crystal engineering field, in which hydrogen bond (HB) has always been of central importance, has garnered even more attention when the XB became part of the crystal engineer toolkit.[15] Indeed, other than being an alternative to the proliferation of supramolecular architectures exclusively built upon HB, the XB possesses a strength comparable to the HB, thus allowing for complementary use to gain a modularity which is unattainable with only strong or weak HB.[16,17] As a consequence, many different promising materials have been developed: porous systems,[18–20] conducting and magnetic materials,[21,22] light responsive polymers and liquid crystals,[23,24] biomimetic materials,[25] and supramolecular gels,[26] are some examples that help to explain why the XB is so appealing to scientists. The medicinal chemistry field may as well benefit from the presence of XB in biological systems: protein-ligand complexes interacting *via* XB have begun to be studied only very recently, with a variety of potential applications spanning from drug discovery to biomolecular recognition.[27,28] Two comprehensive reviews, deeply covering the kaleidoscopic aspects and state-of-the-art of the XB, have been recently published by the groups of Resnati[29] and Beer;[30] the reader is referred to them for more details.

The XB-based crystal engineering strongly relies upon the comprehension of the molecular arrangement in crystals, to design materials with desired properties. Hence, X-ray diffraction (XRD) has traditionally played a crucial role in this field, as it still does.[29] In this context, solid-state nuclear magnetic resonance (SSNMR) has been used either as complementary or alternative technique, providing a wealth of information. For example, it is a site-specific probe of the interaction, possessing the ability to analyze a variety of nuclei; molecular dynamics ranging from GHz to Hz may be studied,[31,32] and quantitative relationships between SSNMR parameters and local structure might also be determined. The most striking difference between SSNMR and XRD is the former's capability of analyzing samples in powder form without any requirement of long-range order. This feature is particularly useful when crystallization problems occur, or when dealing with amorphous or semisolid materials. Moreover, the 'NMR crystallography' approach, which is a combination of SSNMR techniques, computational methods, and powder diffraction, allows the determination of crystal structures which are inaccessible or very difficult to obtain by diffraction methods.[33] Despite all of the advantages, it must be pointed out that the XB characterization by SSNMR is a very challenging task. Difficulties are due to the presence of halogen atoms, which exhibit quadrupolar interaction that causes extremely broad patterns. The problem is usually tackled by using a multinuclear and multiparametric approach, which represents the focus of this highlight. Furthermore, as XB becomes increasingly popular, we deem it advisable to review the importance of SSNMR in this field. We therefore aim to summarize the strategies to successfully probe XBs, unresolved problems, and future directions. This Highlight Article is organized as follow. In section 2 we describe the

Department of Chemistry and NIS centre, University of Torino, Via Pietro Giuria 7, 10125 Torino, Italy. Email: roberto.gobetto@unito.it; Fax: +39 011 6707855; Tel: +39 011 670 7520

basic features of the XB, and outline the strengths and weaknesses of the NMR approach to its characterization. A brief description of the basic SSNMR techniques for measuring the relevant parameters diagnostic of the XB presence is also given here. In section 3 we review the different strategies and applications of SSNMR to characterize the XB, dedicating each paragraph to the key NMR parameters which provide the most valuable information. Finally, an outlook and future perspectives of the relevance of SSNMR in this field are given.

2. Fundamentals

A typical XB occurs between a region of positive electrostatic potential of a polarized halogen atom (X = F, Cl, Br, I) in a molecule R–X and a nucleophilic region of another, or the same, molecular entity (Y).[34,35] A schematic representation of the XB is shown in Fig. 1.

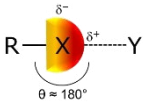

Fig. 1 Typical halogen-bond geometry, where R = C, N, O, halogen, X = F, Cl, Br, I, and Y = N, O, S, Se, I^-, Br^-, Cl^-, F^-, … The red-colored area is a graphical representation of the σ-hole.[29,30]

The exact nature of R–X···Y interactions is still a matter of debate, yet the XB community accepts the so-called "σ-hole model" as the rationale behind the counterintuitive electrophilic behavior of halogens when involved in such interaction.[36] XBs are commonly described in terms of normalized contact, N_c, calculated as the ratio $D_{XY} / (r_x + r_y)$, where D_{XY} is the experimental distance between the halogen atom X and the atom on the acceptor moiety, and r_x, r_y are the corresponding van der Waals radii. The N_c parameter may be used as indicator of the XB strength,[29] and also allows contacts of chemically different interacting sites to be directly compared. The existence of R–X···Y interactions has been traditionally investigated by spectroscopic and diffraction techniques; among others, XRD, infrared, and NMR spectroscopy are the most commonly employed to study the interaction. Solution NMR spectroscopy has long demonstrated to be a convenient and sensitive tool to establish the occurrence of XB, to rank the ability of XB donors and acceptors to be involved in the interaction, and even to describe thermodynamics and geometric features of adducts.[4,37–43] By contrast, detailed studies on XB by SSNMR have been carried out only in recent years. This technique already proved to be a powerful and versatile method for probing HB networks, inasmuch as they required accurate localization of hydrogen atoms.[44–48] Such structural information was by far more precise than the one obtainable by diffraction methods,[33] thus emphasizing the helpfulness of SSNMR to the study of intermolecular interactions. Likewise, the XB affects the NMR observables of nuclei in both the halogen donor (R–X) and the acceptor (Y);[34] however, even if all of the three atoms involved in the interaction are in principle amenable to be studied by NMR, halogen atoms are not easily probed. The NMR active isotopes of halogens possess quantum spin numbers greater than ½: $^{35/37}$Cl, $^{79/81}$Br and ^{127}I are all quadrupolar nuclei. Consequently, a non-spherical charge distribution is present at the nucleus, quantified by the nuclear electric quadrupole moment (Q). The quadrupolar interaction (QI) stems from the interaction between Q and the surrounding electric field gradient (EFG), which is in turn generated by the distribution of charges in the system.[49,50] Hence, high-symmetry atomic environments are associated with small QI, whereas sites of low symmetry give rise to strong QI, which will affect the NMR spectrum with very broad and distorted lineshapes (*vide infra*). For this reason, SSNMR studies on XB are focused mainly on probing the atoms in the R and Y moieties, thereby obtaining indirect evidence of the occurrence of the interaction. In the great majority of X-bonded molecular solids the donor bears a carbon atom directly bonded to the halogen, whereas nitrogen compounds are the most used XB acceptors, followed by oxygen and sulphur compounds.[29] Therefore, ^{13}C and ^{15}N are the most investigated nuclei, and more importantly, their acquisition and interpretation is relatively straightforward. Other spin-½ nuclei such as ^{1}H, ^{19}F, ^{31}P, ^{77}Se have also been reported for either direct or indirect XB characterization. For halogen nuclei, only a handful of data have been published so far, for the reasons mentioned above. Table 1 summarizes the nuclei of interest for SSNMR spectroscopy that may be present in the structural unit of the XB.

Table 1 Summary of nuclei amenable to study by NMR in the three fragments of the XB.

R, (spin)	X, (spin)	Y, (spin)
^{1}H (1/2)	$^{35/37}$Cl (3/2)	^{14}N (1)
^{13}C (1/2)	$^{79/81}$Br (3/2)	^{15}N (1/2)
^{19}F (1/2)	^{127}I (5/2)	^{31}P (1/2)
^{31}P (1/2)		^{77}Se (1/2)
^{14}N (1)		$^{35/37}$Cl (3/2)
^{15}N (1/2)		$^{79/81}$Br (3/2)
		^{127}I (5/2)

2.1 Essential experimental techniques

In order to understand how the useful information is extracted from the vast and rather complicated NMR parameters space, a basic approach to sample characterization is given in this paragraph.

The common SSNMR experiment is carried out on a powdered sample, without any particular requirement about crystallinity, or particle size. On the other hand, a crystalline sample is usually preferable, due to a better spectral resolution than amorphous or disordered samples. This naturally leads us to pinpoint an important feature of SSNMR experiments, that is, the dependence of crystallites on the orientation in the applied magnetic field (B_0). In a powder sample, all orientations are possible; in other words, the spectrum is dominated by spatial-dependent (*i.e.*, anisotropic) interactions, namely the shielding anisotropy, the dipolar coupling, and the quadrupolar interaction which give broad, complex signals. These anisotropic effects are removed by particular techniques, which are crucial to obtain high-quality spectra from powder samples.

Magic-angle spinning (MAS) is routinely used for the primary task of removing CSA effects, and helps in reducing both homo- and heteronuclear dipolar coupling effects. It also assists in narrowing lines from quadrupolar nuclei.[51] MAS is performed by fast rotating (10 to 100 kHz, determined by the rotor diameter) the sample at an angle of 54.74° with respect to the applied magnetic field. MAS provides a single line at the isotropic chemical shift if the spinning rate is fast enough, and anisotropies are small relative to the spinning rate. If spinning is slower, a set of spinning sidebands for each isotropic chemical shift will appear in the spectrum, spaced at integer multiples of the spinning speed.

Dipolar couplings between ^{1}H and other nuclei are generally very intense in the solid-state (up to 50 kHz);[52] therefore, they are eliminated through a high-power proton decoupling (HPPD). Since scalar couplings between protons and other nuclei are weaker than dipolar ones, HPPD eliminates them as well.

The difficulty of long relaxation times for dilute spins (*e.g.* ^{13}C, ^{15}N, ^{31}P) in solids is overcome by cross polarization (CP). This technique allows the transfer of magnetization from abundant spins (*e.g.* ^{1}H, ^{19}F) to the dilute ones, thereby reducing the actual relaxation times and improving signal intensity. The vast majority of powder spectra is today acquired with the CPMAS technique (including of course the HPPD in the pulse sequence), a widespread, standard methodology in the NMR laboratory.

Quadrupolar interactions should be tackled with a tailored approach to the system being studied. For small quadrupolar interactions only first-order perturbation to the Zeeman levels can be considered, and MAS may suffice in averaging to zero the anisotropy, assuming the sample spinning speed is significantly higher than the anisotropic broadening. For large quadrupolar interactions, where also second-order effects dominate the lineshape, MAS is unable to remove the anisotropic effects. Thus, special techniques and hardware are necessary: double rotation (DOR), dynamic angle spinning (DAS), multiple quantum MAS (MQMAS) and satellite transition MAS (STMAS) yield high-resolution spectra of quadrupolar nuclei.

Lastly, it should be noted that while all of these interactions interfere with the observation of individual sites, they provide valuable additional structural information.[33,50] Hence, methods are available for recovering specific couplings that would be otherwise removed, so that important parameters such as internuclear distances,[53–55] J couplings,[56,57] and the quadrupolar coupling constant[50,58] can be determined. For more details on these techniques we refer the readers to refs. 52–58.

3. SSNMR strategies to study the XB

In this section we outline the main literature reports in order to describe the impact of SSNMR in the XB characterization. This part is divided into paragraphs to list the main NMR items for investigating the XB: chemical shifts, dipolar interaction, J-coupling, quadrupolar interaction.

3.1 Chemical shift

SSNMR chemical shift is a sensitive parameter to detect the occurrence and geometry of XB. Indeed, XB formation leads to substantial changes in the isotropic chemical shifts of atoms directly involved or in close proximity of the non-covalent interaction. Moreover, chemical shift positions are a source of information about molecular structure, and may also be used to determine the number of molecules in the asymmetric unit. Rather than its isotropic value, the full chemical shift tensor is a more sensitive probe of the electric surroundings of the atom concerned: the acquisition of static or low-speed MAS spectra allows the measurement of the principal components of the chemical shift tensor, which have been demonstrated to be strongly affected by XB occurrence. In addition, if tensor orientation is known, one may draw precise structural conclusion regarding the geometry of the interaction.

As stated above, the XB donor is often composed of a halogen atom directly bonded to a carbon atom, and the XB acceptor is usually another carbon-rich molecule. Hence, ^{13}C is a convenient probe of the interaction. Its low natural abundance (1.1%) and long relaxation times are easily overcome by the CP technique. If CP is not feasible, due to the lack of adjacent and suitable nuclei from which polarization transfer occurs, one can always rely upon direct excitation experiments. In literature, XB studies by ^{13}C SSNMR focus on the carbon atoms in both the donor and acceptor fragments; however, while the changes in the $\delta_{iso}(^{13}C)$ of several acceptors have been reported to be in the range of 1–3 ppm,[59,60] the extent of the shift is much wider from the donor point of view (Fig. 2).

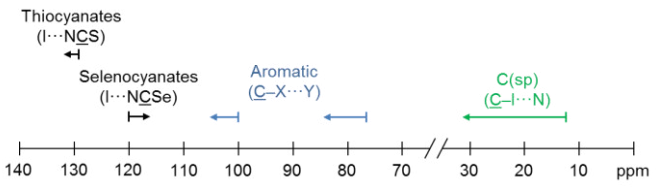

Fig. 2 Schematic representation of XB-induced changes in ^{13}C SSNMR chemical shifts. The difference in the shift direction noted for the selenocyanates may be attributed to an interplay of competing factors that influence the isotropic chemical shift, which are difficult to define univocally. The changes are referred to carbon atoms of either the acceptor (black), or the donor (blue and green). Data are from refs. 59, 60, 64, 71, 72.

Indeed, Bryce and co-workers explored the changes in the $\delta_{iso}(^{13}C)$ of several different XB donors when involved in an XB interaction. They probed the carbons covalently bonded to the halogen atom (C–I) of 1,4-diiodotetrafluorobenzene (p-DITFB), 1,2-diiodotetrafluorobenzene (o-DITFB) and 1,4-diiodobenzene (DIB) co-crystallized with ammonium or phosphonium halide salts.[61,62] Meaningful increases up to 10 ppm were observed in the $\delta_{iso}(^{13}C)$ values of the C–I resonance upon the formation of a XB. The authors also reported a correlation between $\delta_{iso}(^{13}C)$ values and the C–I distance for the p-DITFB co-crystals: an increase of the carbon-iodine bond length corresponds to an increase of the chemical shift. This general trend was corroborated by density functional theory (DFT) calculations, including the zero-order regular approximation (ZORA) to take into account scalar and spin-orbit relativistic effects.[63] Oddly, experimental correlation with the N_c parameter was not observed, perhaps due to the strikingly different crystalline environments considered.

The correlation between the $\delta_{iso}(^{13}C)$ values and the C–I distance in X-bonded co-crystals has been confirmed in our laboratory: we have included iodoperfluoroalkanes into the study, in order to comprise both aromatic and aliphatic sp^3 carbons, thereby giving a better overview of the relationship.[64] In this Highlight, we have tried to further expand the dataset by considering the available $\delta_{iso}(^{13}C)$ values in the literature, when the carbon atom is covalently bonded to iodine and the latter is involved in a XB (Table 2). Other criteria applied to data selection were to choose carbons with fluorinated surroundings, with no disorder of the aromatic ring in the crystallographic structure, and unambiguous assignment of the resonances. Notably, the correlation of the $\delta_{iso}(^{13}C)$ with the C–I distance is very good (R^2 = 0.9727), even though these systems are quite different from each other (Fig. 3). This might be an additional evidence of the robustness of the relationship.

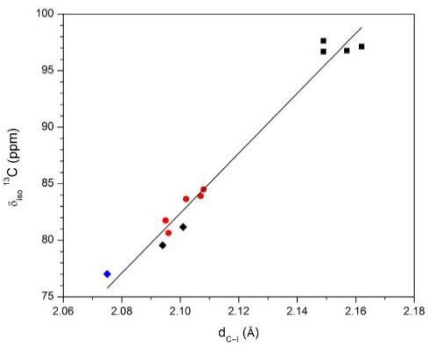

Fig. 3 Plot of experimental values of ^{13}C chemical shift of carbons covalently bonded to iodine. The values are taken from Table 2. The diamonds and the red circles, reported in ref. 64 and 61, respectively, represent X-bonded co-crystals in which the XB donor is p-DITFB. The blue diamond is pure p-DITFB. The black squares represent X-bonded co-crystals in which the XB donor is either diiodoperfluorooctane or diiodoperfluorohexane. The best fit is represented by a linear function: δ_{iso} ^{13}C = 264.97d_{C-I} – 474.05, R^2 = 0.9727.‡ See Table 2 and Footnotes section for further details regarding the dataset.

Table 2 Selected isotropic ^{13}C chemical shifts of carbons covalently bonded to iodine available in the literature, with corresponding C–I distances from X-ray crystallography.

XB type	Compound[a]	δ_{iso} ^{13}C (ppm)	d_{C-I} (Å)	Refs.
	p-DITFB	77.0	2.075	64
C(sp^2)–I···N	[(4,4'-bipy)·(p-DITFB)]	79.6	2.094	64
C(sp^2)–I···N	[(bipyet)·(p-DITFB)]	81.2	2.101	64
C(sp^3)–I···N	[(4,4'-bipy)·($C_8F_{16}I_2$)]	97.1	2.162	64
C(sp^3)–I···N	[(bipyet)·($C_8F_{16}I_2$)]	96.7	2.149	64
C(sp^3)–I···N	[(4,4'-bipy)·($C_6F_{12}I_2$)]	97.6	2.149	64
C(sp^3)–I···N	[(bipyet)·($C_6F_{12}I_2$)]	96.8	2.157	64
C(sp^2)–I···Cl^-	[(*n*-Bu_4NCl)·(p-DITFB)][b]	83.9	2.107	61
		80.6	2.096	61
C(sp^2)–I···Cl^-	[(*n*-Bu_4PCl)·(p-DITFB)][b]	81.8	2.095	61
		83.7	2.102	61
C(sp^2)–I···Br^-	[($EtPh_3PBr)_2$·(p-DITFB)]	84.5	2.108	61

[a]Abbreviations: 1,4-diiodotetrafluorobenzene (p-DITFB), 4,4'-bipyridine (4,4'-bipy), 1,2-bis(4-pyridyl)ethane (bipyet), 1,8-diiodohexadecafluorooctane ($C_8F_{16}I_2$), 1,6-diiododecafluorohexane ($C_6F_{12}I_2$), tetra-*n*-butylammonium chloride (*n*-Bu_4NCl), tetra-*n*-butylphosphonium chloride (*n*-Bu_4PCl), ethyltriphenylphosphoium bromide ($EtPh_3PBr$). [b]Two distinct carbon sites.

Overall, these studies provided evidence that ^{13}C chemical shifts are sensitive probes of the XB occurrence, and their change upon XB formation is directly and linearly related to the C–I distance, which is in turn an indicator of XB.[34]

It is of interest to note that such ^{13}C SSNMR spectra are challenging because MAS does not entirely average the dipolar coupling between carbon, which is a spin-1/2 nucleus, and iodine, which is a quadrupolar, spin-5/2 nucleus. This type of residual dipolar coupling (RDC) is known to occur[65] for other

quadrupolar spins coupled to ^{13}C, for example ^{14}N, $^{35/37}Cl$, and $^{79/81}Br$. The RDC gives rise to specific broadening and splitting patterns, which have been analytically described in several works.[66–68] In the case of C–I resonances, residual dipolar broadening of the ^{13}C signals is observed without any additional splitting. Furthermore, their ^{13}C chemical shifts are markedly shielded due to a well-known spin–orbit-induced heavy atom effect of iodine;[69,70] this relativistic effect reveals to be very useful for an unambiguous assignment of the chemical shifts of such carbon atoms.

Other studies employed XB donors with sp-hybridized carbons, and found additional indication that the ^{13}C SSNMR chemical shifts usually move toward high frequencies upon XB formation. For example, our group has published[71,72] several $\delta_{iso}(^{13}C)$ values for the C(sp)–I resonance in two pharmaceutical compounds, X-bonded with different acceptors such as 4,4'-bipyridine (4,4'-bipy), 1,2-bis-4(pyridyl)ethane (bipyet) and alkyl ammonium halide salts. In accordance with the previous literature results, we measured an increase in the $\delta_{iso}(^{13}C)$ values upon XB formation, ranging from about 7 to 15 ppm. The ^{13}C CPMAS spectra were performed either with non-quaternary suppression (NQS), or simultaneous-phase inversion during the polarization inversion (CPPISPI). These are both spectral editing techniques: the former removes CH and CH_2 signals from the spectrum, while the latter gives a spectrum where CH signals disappear, CH_2 signals are inverted, and CH_3 and quaternary C are normally positive.[73–75] ^{13}C NQS and CPPISPI allowed us to distinguish easily the carbon resonances, and were crucial to unambiguously assign the chemical shifts of the overlapped C(sp)–I resonances, in particular for one of the two pharmaceutical compounds (namely 3-Iodo-2-propynyl-N-butylcarbamate, IPBC) and its co-crystals (Fig. 4).

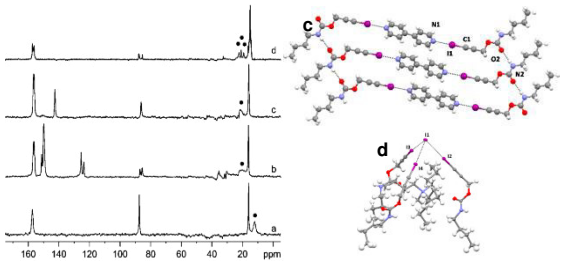

Fig. 4 (Left) ^{13}C (100 MHz) NQS spectra of IPBC (a), and its X-bonded adducts with 1,2-bis-4(pyridyl)ethane, (b) 4,4'-bipyridine (c), and tetrabutylammonium iodide (d). C(sp)–I signals are marked with a black circle. (Right) ball and stick representation of the crystal packing of (c) and (d). Color code: gray, C; red, O; blue, N; purple, I; white; H. (Reproduced with permission from ref. 64. Copyright 2013 American Chemical Society).

Another SSNMR spectral signature of the XB occurrence may be retrieved from nitrogen nuclei. Nitrogen is of high interest for SSNMR studies of XB, as it is often directly involved in the interaction. Therefore, it has been exploited since the very first works[76–79] on XB by SSNMR, although data were sparse and related to a variety of compounds. Efforts towards systematic approaches have been made only in recent times,[59,60,64,71,72] and they succeeded in revealing the potential of nitrogen SSNMR for the XB characterization. Nitrogen has two NMR-active isotopes, though only one is non-quadrupolar, that is, ^{15}N. Unfortunately, ^{15}N has an extremely low natural abundance (0.37%) and small gyromagnetic ratio; therefore, a ^{15}N CPMAS spectrum may require very long accumulation times, up to 15–20 hours (or days at worst), to yield an acceptable signal-to-noise ratio. This sensitivity issue refrains SSNMR spectroscopists from taking up the challenge, although such long data collection may be significantly shortened using ^{15}N-enriched compounds. Besides, isotopic enrichment dramatically reduces the time needed to measure the CSA, thereby obtaining a full description of the tensor and, if conditions are favorable, of the interaction geometry. For example, Bryce and coworkers used a ^{15}N-labeled tetramethylammonium thiocyanate sample to synthesize a X-bonded cocrystal with p-DITFB.[59] They observed a small, but measurable shift of 2.5 ppm to low frequencies of the thiocyanate $\delta_{iso}(^{15}N)$ upon XB formation, and an increase of about 70 ppm in the span value of the ^{15}N CS tensor relatively to the pure compound. Although the ^{15}N CS tensor analysis was successful, the authors were cautious in drawing conclusions due to disorder of the thiocyanate anion, as detected by the increased linewidth of the resonances.

Natural abundance ^{15}N CPMAS has been recently applied in our laboratory for the direct detection of the XB in a systematic study[64] of dipyridyl derivatives, which are commonly employed for assembling X-bonded structures. Specifically, the $\delta_{iso}(^{15}N)$ of 4,4'-bipy and bipyet have been observed to generally move toward low frequencies when forming N···X motifs (X = I, Br), with substantial changes in the order of tens of ppm. Moreover, the $\delta_{iso}(^{15}N)$ values have been shown to nicely correlate with the geometry of the XB, as quantified by the N_c parameter (Fig. 5): when the chemical shift increases, the N_c parameter increases. Interestingly, GIPAW DFT calculations showed general agreement with the experimental correlation (Fig. 6), and, despite some difficulties in comparing different crystal packings, the trend can be used to estimate the XB geometry with affordable natural abundance ^{15}N chemical shift analysis.

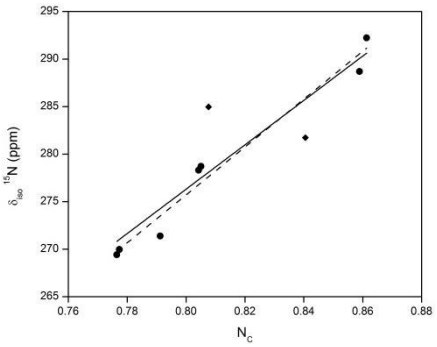

Fig. 5 Plot of the experimental values of ^{15}N isotropic chemical shifts as a function of the corresponding N_c parameter. The diamonds represent two X-bonded co-crystals the space groups of which are different from the others. The solid line represents the best fit including the latter: $\delta_{iso}{}^{15}N = 233.4N_c + 89.6$, $R^2 = 0.8273$. The dashed line represents the best fit excluding them: $\delta_{iso}{}^{15}N = 251.9\ N_c + 74.2$, $R^2 = 0.9650$. Reprinted and adapted with permission from ref. 64. Copyright 2016 John Wiley and Sons.

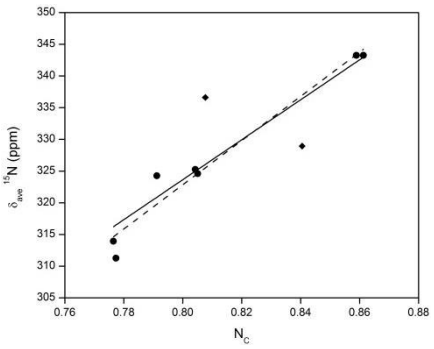

Fig. 6 Plot of the calculated values of ^{15}N isotropic chemical shifts as a function of the corresponding N_c parameter. Reproduced with permission from ref. 64. Copyright 2016 John Wiley and Sons.

Results from systematic XB investigations by ^{15}N SSNMR are outlined in Fig. 7. The encouraging conclusion is that isotropic ^{15}N chemical shifts are sensitive to the XB occurrence in a measurable and meaningful way, certainly more than ^{13}C's. It is of interest to note that this ^{15}N peculiarity had already been observed in the case of HB formation,[80] and also upon metal coordination.[81–84]

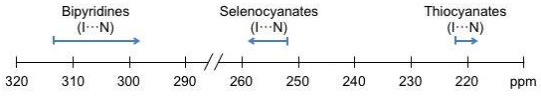

Fig. 7 Schematic representation of XB-induced changes in ^{15}N isotropic chemical shifts. The reason of the opposite behavior of the selenocyanates chemical shifts change upon XB formation is the same already described in Fig. 2. The scale is referenced to liquid NH_3 (i.e., $\delta(^{15}N, NH_3) = 0$ ppm). Data are from refs. 59, 64, 71, 72.

Other spin-1/2 nuclei, somewhat less popular than carbon and nitrogen, have been exploited to study the XB. For example, Viger-Gravel *et al.* applied ^{77}Se SSNMR to the direct detection of XB in selenocyanates complexes with either o- or p-DITFB, exhibiting Se···I motifs.[59] The authors showed that ^{77}Se isotropic chemical shifts move substantially toward high frequencies when XB occurs. Furthemore, CS tensor analysis revealed that the changes of the smallest component of the chemical shift tensor, δ_{33}, which is oriented parallel to the axis of the selenocyanate anion, are related to the perturbations of molecular orbitals in the plane perpendicular to the anion's axis. This plane is that in which iodine engages in XB with the selenium center; for this reason, the authors concluded that δ_{33} value is a good measure of the extent of the XB in Se···I adducts. In a later work,[85] they confirmed the marked sensitivity of ^{77}Se to the XB by reporting increases of ^{77}Se isotropic chemical shifts in a range of about 40 to 100 ppm, for a series of triphenylphosphine selenide co-crystals with iodobenzene derivatives.

Fluorine atoms are purposefully added to the chemical structure of XB donors, since they enhance the σ-hole magnitude, thus allowing XB to be more effective.[30,86] Solution ^{19}F NMR studies have therefore been extensively used to probe XB interactions, due to the large fluorine chemical shift range and sensitivity (natural abundance of 100%).[41] However, ^{19}F NMR in the solid state is technically challenging: strong homonuclear dipolar coupling between ^{19}F nuclei and large CSA require high radiofrequency powers, dedicated hardware, and high spinning speeds. Widdifield *et al*. reported[60] a decrease in the $\delta_{iso}(^{19}F)$ values upon XB formation for complexes of p-DITFB and 1,4-dibromotetrafluorobenzene (p-DBrTFB) with decamethonium diiodide; it is also noted that ^{19}F MAS data were useful to confirm the static disorder as observed in XRD structures. Pérez-Torralba and co-workers reported[87] some $\delta_{iso}(^{19}F)$ values for fluorine-substituted benzimidazoles exhibiting F···F short contacts.

^{31}P is an NMR-active isotope with 100% natural abundance, for which CS tensor analysis has been applied for the indirect detection of XB. The group of Bryce reported[88] consistent increases of about 5–10 ppm of the $\delta_{iso}(^{31}P)$ for triphenylphosphine oxide upon co-crystallization with iodobenzene derivatives. Conversely, the same XB donors caused the $\delta_{iso}(^{31}P)$ to change by the same extent but in the opposite direction for triphenylphosphine selenide samples.[85]

Finally, we complete this overview of spin-1/2 nuclei by noting an application of SSNMR to probe dynamics in the XB: Garcia-Garibay and co-workers used variable-temperature, wide-line ^{1}H experiments to measure the molecular dynamics in X-bonded rotors with potential application as molecular machines.[32,89] The technique is based on the analysis of spin-lattice relaxation times (T_1) as a function of temperature, thereby giving access to the rotational frequencies and activation energies through appropriate mathematical models.

3.1 Dipolar interaction

Dipolar coupling represents the cornerstone of NMR crystallography, because it allows for the measurement of internuclear distances and establishing connectivities. It has been extensively exploited for geometrical and structural elucidation of H-bonded compounds, and therefore has had

pivotal role in the development of the SSNMR for analyzing co-crystals and polymorphs: a review published by our group is available.[53]

Dipolar couplings stem from the interaction of two nuclear spin close in space, which experience each other's magnetic field. It is therefore a through-space interaction, and it scales with the inverse cube of the distance between spin *I* and *S*:

$$D_{IS} = \frac{\mu_0}{4\pi}\frac{\gamma_I \gamma_S \hbar}{r_{IS}^3}$$

where γ_I and γ_S are the gyromagnetic ratios of spins *I* and *S*, and μ_0 is the magnetic permeability constant. Although averaged out in high-resolution spectra (see paragraph 2.1), many recoupling sequences have been developed to reintroduce it in the final spectrum, in order to recover the information. Weingarth *et al.* used rotary resonance recoupling to examine a ^{15}N-enriched benzyl-di(4-iodobenzyl)-amine, that was expected to form N···I intermolecular XB.[90] The experiment required only irradiation of protons and ^{15}N nuclei, in order to determine the dipolar interaction between ^{15}N and ^{127}I; effects due to quadrupolar-dipolar cross-terms, or *J*-coupling anisotropy were safely neglected. The numerical value of *D* as well as the N···I distance were obtained by fitting the rotary resonance lineshapes with simulated ones, which in turn were obtained by experimental CSA parameters (Fig. 8).

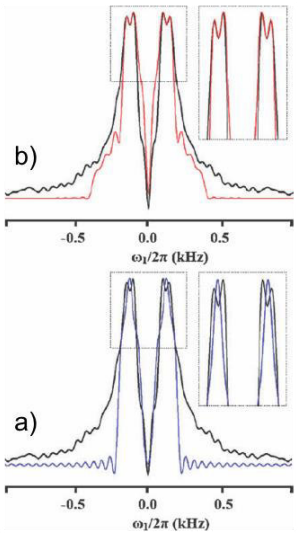

Fig. 8 ^{15}N SSNMR rotary resonance lineshapes (black) in the indirect dimension, along with simulated lineshapes (blue and red). In (a), the simulated lineshape has been obtained by assuming contribution only from the ^{15}N CSA; in (b), the simulated lineshape has been obtained by considering contribution from both the ^{15}N CSA and ^{15}N, ^{127}I dipolar coupling. The simulation parameters afforded the internuclear N···I distance in the benzyl-di(4-iodobenzyl)-amine sample, that is, $d = 2.7 \pm 0.04$ Å. Reproduced with permission from ref. 90. Copyright 2008 The Royal Society of Chemistry.

This method provided a value of the internuclear distance significantly shorter than the sum of the Van der Waals radii, and it is particularly useful when the quality of single crystals is not suitable for XRD analysis.

While many efforts have been devoted to the measurement of HB distances, in the case of XB characterization they have been scarcely applied because they usually require homogeneous excitation of the quadrupolar nucleus, which is not easily achieved. Hopefully, SSNMR spectroscopists will face the challenge in the forthcoming years.

3.3 *J*-coupling

Indirect spin-spin (*J*) couplings provide insight into through-bond connectivities, and depend on the interaction between two bonded nuclear spins and their bonding electrons. *J*-couplings in the solid state are normally not resolved, since their magnitude ($1 - 10^3$ Hz) is of the same order or smaller than the usual linewidth. Nonetheless, 2D SSNMR experiments have been developed to examine chemical bonding *via* *J*-coupling, thus enabling correct assignment of the observed resonances in monodimensional experiments and thorough structure elucidation.[31] More importantly in the context of intermolecular interactions, *J*-couplings mediated by HB have been used to detect N–H···N connectivities in small molecules;[91,92] also, an unusual intermolecular *J*-coupling between non-bonded ^{77}Se and ^{31}P has been recently observed in the solid state by Ashbrook and co-workers.[93]

In the case of XB, Viger-Gravel *et al*. measured the *J*(^{77}Se, ^{31}P) of a triphenylphosphine selenide sample alone and in a series of X-bonded co-crystals with iodobenzene derivatives, exhibiting P=Se···I short contacts.[85] *J*-couplings showed up as a doublet in ^{77}Se CPMAS spectra. J_{iso} values were determined by fitting the experimental lineshapes with simulated ones; a decrease in magnitude as XB weakens was observed. Similarly, Xu *et al.* reported a decrease of J_{iso} between ^{31}P and ^{17}O upon XB formation, by acquiring ^{31}P CPMAS spectra for co-crystals of triphenylphosphine oxide with iodobenzene derivatives, that interact *via* P=O···I motifs.[88] A linear correlation between *J*(^{31}P, ^{17}O) and the N_c parameter was also established by DFT calculations, with scalar relativistic corrections. These early findings suggest that *J*-couplings between nuclei which are in close proximity of the XB are sensitive to the presence of the XB itself; however, future development of the SSNMR technique might enable the measurement of *J*-couplings across the XB, which would possibly be a better indicator of the intermolecular interaction.

3.4 Quadrupolar interaction

Quadrupolar SSNMR techniques would be ideally suited for investigating halogens in XB. However, as stated above, quadrupolar nuclei are extremely challenging and difficult to probe, since QI can be almost equal in magnitude to Zeeman interaction ($10^3 - 10^7$ Hz), thus severely enlarging the breadth

of the spectrum. The NMR spectra of $^{35/37}$Cl, $^{79/81}$Br, and ^{127}I are typically dominated by QI.[94] Basics of QI have been described in section 2; in this paragraph we go further into discussing the methodologies and results of quadrupolar SSNMR applied to the study of the XB.

The QI is analytically described by the quadrupolar coupling constant $C_Q = (eV_{33}Q / h)$ and the asymmetry parameter $\eta_Q = (V_{11} - V_{22}) / V_{33}$, where $|V_{33}| \geq |V_{22}| \geq |V_{11}|$ are the principal components of the EFG tensor. Typical values of C_Q are in the order of 10^1 - 10^3 MHz, whereas η_Q values range from zero to one. Quadrupolar SSNMR experiments yield these two parameters, in addition to the CS of the observed nucleus, thus providing insights into the local and electronic structure and symmetry. The Q value for halogens range from moderate ($^{35/37}$Cl) to high (^{127}I); therefore, the QI is often too large even for the mere acquisition of the spectrum, unless the halogen lay on a site with high symmetry. Hence, the great majority of SSNMR studies of chlorine, bromine, and iodine has been focused on observing the more accessible anionic forms of these elements, rather than covalently-bonded halogens.[94] The first direct observation of ^{35}Cl SSNMR spectra of a covalently-bonded chlorine engaged in XB has been very recently performed by Szell *et al.*[95] They probed Cl···N contacts in several small organic molecules using WURST-QCPMG sequence[50] at 21.1 T, corroborating the numerical values of C_Q and η_Q with ^{35}Cl NQR spectroscopy. This method was sensitive to small changes in the EFG caused by XB, as verified by natural localized molecular orbital analysis (NLMO), and also allowed resolution of multiple chlorine sites in the powder spectrum (Fig. 9).

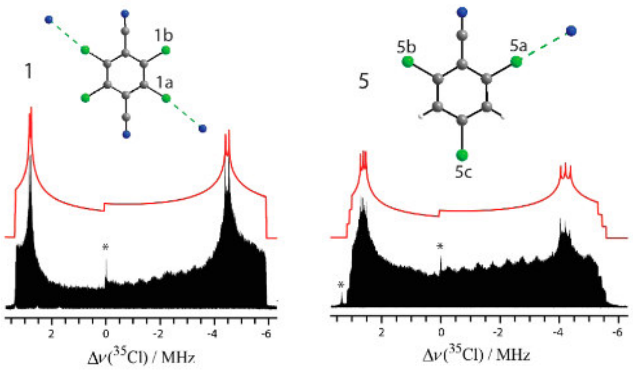

Fig. 9. Selected ^{35}Cl SSNMR spectra (21.1 T) from ref. 95 of tetrachloroterephtalonitrile (1), and 2,4,6-trichlorobenzonitrile (5). Red traces are spectral simulations. The asterisks denote interference from local radio stations, and trace NaCl, used as chemical shift reference. Numbers on atoms denote nonequivalent crystallographic chlorines. Reprinted and adapted with permission from ref. 95. Copyright 2016 American Chemical Society.

The first example of XB investigation by ^{35}Cl, ^{81}Br, and ^{127}I SSNMR was reported in an early work by Bryce and co-workers.[96] A full analysis of the CS, CSA, and quadrupolar parameters, carried out on a series of haloanilinium halides, showed the importance of the EFG in describing the XB environment: in particular, the C_Q of a chloride anion may be used to differentiate between two distinct ion coordination environments. Moreover, smaller δ_{iso}(^{81}Br) and ^{81}Br span were observed when XB became weaker. SSNMR data for ^{127}I were also reported by Widdiefield *et al.* for iodides involved in I^-···I XBs.[60] High difficulties were encountered in collecting such spectra, even at ultra-high magnetic fields; the authors concluded that the XB creates such a distortion about the halide so as to render the acquisition of ^{127}I SSNMR impractical with current technology. Other reports deal with the relationships between quadrupolar SSNMR parameters and the XB environment: for example, a clear correlation was established between the η_Q value of either ^{35}Cl or ^{81}Br and the I···X^-···I angle, for a broad range of geometries.[62] This result is in qualitative agreement with previous corresponding data available for the HB. The first ^{17}O MAS NMR study was reported by Xu *et al.*,[88] for ^{17}O- labeled co-crystals featuring P=O···I–C XBs. The authors found both C_Q and η_Q to increase upon XB formation, confirming once again the sensitivity of quadrupolar parameters to the variations in the electronic structure of halogens due to XB.

At this point, it is noteworthy that the examination of the QI through SSNMR experiments is a formidable task, whereas the calculation of quadrupolar NMR parameters demands little computational cost.[93] The presence of nuclei with large atomic number requires the inclusion of relativistic effects for an accurate description of magnetic shielding tensors;[97] at the same time, in a solid-state calculation one needs to consider the crystalline nature of the material, thus accounting for the long-range electrostatic effects of the crystal lattice.[98] To date, a fully-relativistic implementation of the GIPAW method is still not available. A simple scalar relativistic approach is however possible, though few examples have been reported.[99,100] In the specific case of XB, quantum chemical calculations of SSNMR parameters are carried out on both cluster models and periodic systems. It has not yet been quantified whether one method is better than the other, although Viger-Gravel *et al.* verified that the inclusion of relativistic corrections for a particular kind of X-bonded co-crystals was more critical than the inclusion of periodic boundary conditions.[61] It would be desirable to adopt a fully-relativistic treatment in concert with GIPAW method, so that both spin–orbit and long-range effects from the crystal packing are simultaneously taken into account. This would help to define the relationships between X-bonded crystal structures and SSNMR parameters in a proper and accurate manner.

Lastly, a possible alternative approach, which has yet to be evaluated thoroughly, may be nuclear quadrupole resonance (NQR) spectroscopy. It enables direct detection of quadrupolar nuclei involved in XB without requiring any external magnetic field. Hence, the absence of a Zeeman interaction ensures that only QI is present; the other interactions are generally too weak to be observed.[101] Pure NQR measurements provide the quadrupolar frequency ν_Q, and the full quadrupole coupling tensor; however, in the case of spin-3/2 nuclei, only a single quadrupolar frequency can be obtained, which is insufficient

to determine the values of C_Q and η_Q. Techniques are available to overcome the problem, such as the addition of a weak magnetic field, or 2D nutation experiments.[102,103] Some old NQR studies on XB have been reported, wherein changes in the quadrupolar frequency upon XB formation were observed.[104–107]

Conclusions and outlook

This Highlight article has provided an overview of the capabilities of SSNMR in characterizing the XB. The variety of the presented SSNMR techniques shows how information on XB is obtained, and also represents an excellent approach complementary to diffraction. In view of the possible future applications of the XB as driving force to assemble functional materials, one can envisage using SSNMR in concert with diffraction and computation to fully understand the solid-state structure at both long- and short-range level. Such approach enables a robust, detailed picture of the material, and ultimately cancels out limitations and disadvantages inherent in each technique. This is the main reason for which SSNMR methodologies should be considered when a XB characterization is needed. The reader should be now aware that the utility of SSNMR goes beyond the simple XB detection: we have shown many examples wherein small changes in local structure caused by XB are revealed by SSNMR, and these changes are quantitatively related to strength and geometry. Other noteworthy points of interest are the ability in studying dynamics at different timescales in molecular rotors, the discrimination among nonequivalent crystallographic sites, and the measurement of internuclear distances. The latter in particular needs further work in order to expand and promote the use of SSNMR in the XB field. Indeed, the measurement of X···Y distance at natural isotopic abundance would be a giant step forward, especially from an NMR crystallography perspective.

SSNMR analysis of XB strongly relies upon spectral simulations for obtaining a full description of tensor quantities, and quantum chemical computations are of great aid for relating structural features with experimental spectra. However, there is need for improvement in the computational methods: the inclusion of relativistic corrections in the calculation of NMR parameters has been implemented only for cluster models, for which long-range effects are evidently overlooked. On the other hand, the accuracy of periodic DFT calculations in describing solid-state systems is ruled out by the lack of a full relativistic treatment. Spin–orbit coupling critically affects not only the shielding of halogen nuclei themselves, but also the shielding of nearby light nuclei: we recall here the case of carbons bonded to iodine. Hence, for XB in particular, it is important to take into account relativistic effects, thereby improving the consistency and the precision of the fits between calculated and experimental data.

A major challenge is represented by the direct observation of halogen nuclei. Chlorine, bromine, and iodine SSNMR, especially when these nuclei are in covalent bond environments, is still very far from routine, if not impractical; however, as technology advances, quadrupolar SSNMR experiments of such species are becoming realistic. We are today witnessing impressive developments of the SSNMR technology: higher magnetic fields, ultra-fast MAS rates, sophisticated hardware for accurate and powerful radiofrequency pulses make it feasible to perform complex multi-dimensional, multi-channel experiments which were inconceivable only a few years ago. NMR spectroscopists are already working in this direction, and the XB could boost major improvements of the technique. NQR is perhaps better suited for addressing the problem of halogen nuclei observation, although additional evidence is needed. The intrinsic difficulty in searching for the quadrupolar frequency has probably limited the application of NQR to XB investigation, yet it remains an excellent experimental method for obtaining a full description of the quadrupole coupling tensor.

On balance, the arsenal of SSNMR techniques provides detailed structural information on the XB, and offers alternative means to understand and control the properties of the materials of interest. If realized as envisaged, future perspectives would further expand the role of SSNMR as essential characterization technique in the XB field and in the crystal engineering in general.

Acknowledgements

P.C.V. thanks the Istituto Nazionale della Previdenza Sociale (INPS) for a scholarship. The authors are indebted with Jeol Company for helpful technical assistance and cooperation.

Notes and references

‡The p-DITFB point in Fig. 3 was previously reported with an erroneous C–I distance, leading to an exponential correlation with the isotropic ^{13}C chemical shifts (see ref. 61). The same crystallographic structure (ZZZAVM01) by Chaplot *et al.*[108] has been used in the present contribution, leading to a linear fit even with the inclusion of distinct compounds from different laboratories.

1 A. Priimagi, G. Cavallo, P. Metrangolo and G. Resnati, *Acc. Chem. Res.*, 2013, **46**, 2686–2695.
2 P. Metrangolo and G. Resnati, *Cryst. Growth Des.*, 2012, **12**, 5835–5838.
3 A. C. Legon, *Angew. Chem., Int. Ed.*, 1999, **38**, 2687–2714.
4 P. Metrangolo and G. Resnati, *Chem. – Eur. J.*, 2001, **7**, 2511–2519.
5 P. Metrangolo, H. Neukirch, T. Pilati and G. Resnati, *Acc. Chem. Res.*, 2005, **38**, 386–395.
6 P. Metrangolo, F. Meyer, T. Pilati, G. Resnati and G. Terraneo, *Angew. Chem., Int. Ed.*, 2008, **47**, 6114–6127.
7 G. Cavallo, P. Metrangolo, T. Pilati, G. Resnati, M. Sansotera and G. Terraneo, *Chem. Soc. Rev.*, 2010, **39**, 3772–3783.
8 G. Cavallo, P. Metrangolo, T. Pilati, G. Resnati and G. Terraneo, in *Halogen Bonding I: Impact on Materials Chemistry and Life Sciences*, eds. P. Metrangolo and G. Resnati, Springer-Verlag Berlin, Berlin, 2015, vol. 358, pp. 1–17.

9 S. Schindler and S. M. Huber, in *Halogen Bonding II: Impact on Materials Chemistry and Life Sciences*, eds. P. Metrangolo and G. Resnati, Springer-Verlag Berlin, Berlin, 2015, vol. 359, pp. 167–203.
10 A. V. Jentzsch, *Pure Appl. Chem.*, 2015, **87**, 15–41.
11 A. C. Legon, *Phys. Chem. Chem. Phys.*, 2010, **12**, 7736–7747.
12 G. Berger, J. Soubhye and F. Meyer, *Polym. Chem.*, 2015, **6**, 3559–3580.
13 R. Wilcken, M. O. Zimmermann, A. Lange, A. C. Joerger and F. M. Boeckler, *J. Med. Chem.*, 2013, **56**, 1363–1388.
14 M. R. Scholfield, C. M. Vander Zanden, M. Carter and P. S. Ho, *Protein Sci.*, 2013, **22**, 139–152.
15 G. R. Desiraju, *J. Am. Chem. Soc.*, 2013, **135**, 9952–9967.
16 A. Mukherjee, *Cryst. Growth Des.*, 2015, **15**, 3076–3085.
17 A. Mukherjee, S. Tothadi and G. R. Desiraju, *Acc. Chem. Res.*, 2014, **47**, 2514–2524.
18 J. Lieffrig, O. Jeannin and M. Fourmigue, *J. Am. Chem. Soc.*, 2013, **135**, 6200–6210.
19 H. Takezawa, T. Murase, G. Resnati, P. Metrangolo and M. Fujita, *Angew. Chem., Int. Ed.*, 2015, **54**, 8411–8414.
20 K. Raatikainen and K. Rissanen, *CrystEngComm*, 2011, **13**, 6972–6977.
21 K.-S. Shin, M. Brezgunova, O. Jeannin, T. Roisnel, F. Camerel, P. Auban-Senzier and M. Fourmigue, *Cryst. Growth Des.*, 2011, **11**, 5337–5345.
22 H. M. Yamamoto, Y. Kosaka, R. Maeda, J. Yamaura, A. Nakao, T. Nakamura and R. Kato, *Acs Nano*, 2008, **2**, 143–155.
23 A. Priimagi, G. Cavallo, A. Forni, M. Gorynsztejn-Leben, M. Kaivola, P. Metrangolo, R. Milani, A. Shishido, T. Pilati, G. Resnati and G. Terraneo, *Adv. Funct. Mater.*, 2012, **22**, 2572–2579.
24 D. W. Bruce, P. Metrangolo, F. Meyer, T. Pilati, C. Praesang, G. Resnati, G. Terraneo, S. G. Wainwright and A. C. Whitwood, *Chem. – Eur. J.*, 2010, **16**, 9511–9524.
25 S. Samai and K. Biradha, *CrystEngComm*, 2009, **11**, 482–492.
26 L. Meazza, J. A. Foster, K. Fucke, P. Metrangolo, G. Resnati and J. W. Steed, *Nat. Chem.*, 2013, **5**, 42–47.
27 Z. Xu, Z. Yang, Y. Liu, Y. Lu, K. Chen and W. Zhu, *J. Chem. Inf. Model.*, 2014, **54**, 69–78.
28 P. S. Ho, in *Halogen Bonding I: Impact on Materials Chemistry and Life Sciences*, eds. P. Metrangolo and G. Resnati, Springer-Verlag Berlin, Berlin, 2015, vol. 358, pp. 241–276.
29 G. Cavallo, P. Metrangolo, R. Milani, T. Pilati, A. Priimagi, G. Resnati and G. Terraneo, *Chem. Rev.*, 2016, **116**, 2478–2601.
30 L. C. Gilday, S. W. Robinson, T. A. Barendt, M. J. Langton, B. R. Mullaney and P. D. Beer, *Chem. Rev.*, 2015, **115**, 7118–7195.
31 S. P. Brown, *Macromol. Rapid Commun.*, 2009, **30**, 688–716.
32 C. Lemouchi, C. S. Vogelsberg, L. Zorina, S. Simonov, P. Batail, S. Brown and M. A. Garcia-Garibay, *J. Am. Chem. Soc.*, 2011, **133**, 6371–6379.
33 R. K. Harris, R. E. Wasylishen and M. J. Duer, Eds., *NMR Crystallography*, John Wiley & Sons, Ltd, Chichester, 2009.
34 G. R. Desiraju, P. S. Ho, L. Kloo, A. C. Legon, R. Marquardt, P. Metrangolo, P. Politzer, G. Resnati and K. Rissanen, *Pure Appl. Chem.*, 2013, **85**, 1711–1713.
35 P. Politzer, J. S. Murray and T. Clark, *Phys. Chem. Chem. Phys.*, 2010, **12**, 7748–7757.
36 M. H. Kolar and P. Hobza, *Chem. Rev.*, 2016, **116**, 5155–5187.
37 P. Cardillo, E. Corradi, A. Lunghi, S. Valdo Meille, M. Teresa Messina, P. Metrangolo and G. Resnati, *Tetrahedron*, 2000, **56**, 5535–5550.
38 A. De Santis, A. Forni, R. Liantonio, P. Metrangolo, T. Pilati and G. Resnati, *Chem. – Eur. J.*, 2003, **9**, 3974–3983.
39 S. Libri, N. A. Jasim, R. N. Perutz and L. Brammer, *J. Am. Chem. Soc.*, 2008, **130**, 7842–7844.
40 E. Dimitrijević, O. Kvak and M. S. Taylor, *Chem. Commun.*, 2010, **46**, 9025–9027.
41 M. G. Sarwar, B. Dragisic, L. J. Salsberg, C. Gouliaras and M. S. Taylor, *J. Am. Chem. Soc.*, 2010, **132**, 1646–1653.
42 A.-C. C. Carlsson, J. Grafenstein, A. Budnjo, J. L. Laurila, J. Bergquist, A. Karim, R. Kleinmaier, U. Brath and M. Erdelyi, *J. Am. Chem. Soc.*, 2012, **134**, 5706–5715.
43 R. A. Thorson, G. R. Woller, Z. L. Driscoll, B. E. Geiger, C. A. Moss, A. L. Schlapper, E. D. Speetzen, E. Bosch, M. Erdelyi and N. P. Bowling, *Eur. J. Org. Chem.*, 2015, 1685–1695.
44 M. U. Schmidt, J. Bruening, J. Glinnemann, M. W. Huetzler, P. Moerschel, S. N. Ivashevskaya, J. van de Streek, D. Braga, L. Maini, M. R. Chierotti and R. Gobetto, *Angew. Chem., Int. Ed.*, 2011, **50**, 7924–7926.
45 M. R. Chierotti, L. Ferrero, N. Garino, R. Gobetto, L. Pellegrino, D. Braga, F. Grepioni and L. Maini, *Chem. – Eur. J.*, 2010, **16**, 4347–4358.
46 S. D. Gumbert, M. Koerbitzer, E. Alig, M. U. Schmidt, M. R. Chierotti, R. Gobetto, X. Li and J. van de Streek, *Dyes Pigments*, 2016, **131**, 364–372.
47 M. R. Chierotti, R. Gobetto, C. Nervi, A. Bacchi, P. Pelagatti, V. Colombo and A. Sironi, *Inorg. Chem.*, 2014, **53**, 139–146.
48 M. R. Chierotti and R. Gobetto, *Chem. Commun.*, 2008, 1621–1634.
49 C. M. Widdifield, R. P. Chapman and D. L. Bryce, *Annu. Rep. NMR Spectrosc.*, 2009, **66**, 195–326.
50 C. Fernandez and M. Pruski, in *Solid State NMR*, ed. J. C. C. Chan, Springer-Verlag Berlin, Berlin, 2012, vol. 306, pp. 119–188.
51 M. J. Duer, *Solid State NMR Spectroscopy: Principles and Applications*, Wiley-Blackwell, Oxford, 2002.
52 D. C. Apperley, R. K. Harris and P. Hodgkinson, *Solid-State NMR: Basic Principles and Practice*, Momentum Press, New York, 2012.
53 M. R. Chierotti and R. Gobetto, *CrystEngComm*, 2013, **15**, 8599–8612.
54 N. C. Nielsen, L. A. Strasso and A. B. Nielsen, in *Solid State NMR*, ed. J. C. C. Chan, Springer-Verlag Berlin, Berlin, 2012, vol. 306, pp. 1–45.
55 G. Tricot, J. Trebosc, F. Pourpoint, R. Gauvin and L. Delevoye, *Annu. Rep. NMR Spectrosc.,* 2014, **81**, 145–184.
56 A. Lesage, in *NMR Crystallography*, eds. R. K. Harris, R. E. Wasylishen and M. J. Duer, John Wiley & Sons, Ltd, Chichester, 2009, pp. 209–222.
57 I. Bertini, L. Emsley, I. C. Felli, S. Laage, A. Lesage, J. R. Lewandowski, A. Marchetti, R. Pierattelli and G. Pintacuda, *Chem. Sci.*, 2011, **2**, 345–348.
58 S. E. Ashbrook and S. Wimperis, *Prog. Nucl. Magn. Reson. Spectrosc.*, 2004, **45**, 53–108.
59 J. Viger-Gravel, I. Korobkov and D. L. Bryce, *Cryst. Growth Des.*, 2011, **11**, 4984–4995.
60 C. M. Widdifield, G. Cavallo, G. A. Facey, T. Pilati, J. Lin, P. Metrangolo, G. Resnati and D. L. Bryce, *Chem. – Eur. J.*, 2013, **19**, 11949–11962.
61 J. Viger-Gravel, S. Leclerc, I. Korobkov and D. L. Bryce, *CrystEngComm*, 2013, **15**, 3168–3177.
62 J. Viger-Gravel, S. Leclerc, I. Korobkov and D. L. Bryce, *J. Am. Chem. Soc.*, 2014, **136**, 6929–6942.

63 E. van Lenthe, J. G. Snijders and E. J. Baerends, *J. Chem. Phys.*, 1996, **105**, 6505–6516.
64 P. Cerreia Vioglio, L. Catalano, V. Vasylyeva, C. Nervi, M. R. Chierotti, G. Resnati, R. Gobetto and P. Metrangolo, *Chem. – Eur. J.*, 2016, DOI: 10.1002/chem.201603392.
65 S. Wi and L. Frydman, *J. Chem. Phys.*, 2000, **112**, 3248–3261.
66 A. Olivieri, *J. Magn. Reson.*, 1989, **81**, 201–205.
67 A. Aliev, K. Harris, R. Harris, S. Carss and A. Olivieri, *J. Chem. Soc., Faraday Trans.*, 1995, **91**, 3167–3176.
68 C. Pettinari, C. di Nicola, F. Marchetti, R. Pettinari, B. W. Skelton, N. Somers, A. H. White, W. T. Robinson, M. R. Chierotti, R. Gobetto and C. Nervi, *Eur. J. Inorg. Chem.*, 2008, **2008**, 1974–1984.
69 R. Glaser, N. Chen, H. Wu, N. Knotts and M. Kaupp, *J. Am. Chem. Soc.*, 2004, **126**, 4412–4419.
70 M. Kaupp, O. L. Malkina, V. G. Malkin and P. Pyykko, *Chem. – Eur. J.*, 1998, **4**, 118–126.
71 M. Baldrighi, G. Cavallo, M. R. Chierotti, R. Gobetto, P. Metrangolo, T. Pilati, G. Resnati and G. Terraneo, *Mol. Pharm.*, 2013, **10**, 1760–1772.
72 M. Baldrighi, D. Bartesaghi, G. Cavallo, M. R. Chierotti, R. Gobetto, P. Metrangolo, T. Pilati, G. Resnati and G. Terraneo, *CrystEngComm*, 2014, **16**, 5897–5904.
73 X. Wu and K. Zilm, *J. Magn. Reson. A*, 1993, **102**, 205–213.
74 X. Wu and K. Zilm, *J. Magn. Reson. A*, 1993, **104**, 119–122.
75 X. Wu, S. Burns and K. Zilm, *J. Magn. Reson. A*, 1994, **111**, 29–36.
76 K. Bouchmella, S. G. Dutremez, B. Alonso, F. Mauri and C. Gervais, *Cryst. Growth Des.*, 2008, **8**, 3941–3950.
77 M. Ángeles García, P. Cabildo, R. M. Claramunt, E. Pinilla, M. Rosario Torres, I. Alkorta and J. Elguero, *Inorg. Chim. Acta*, 2010, **363**, 1332–1342.
78 C. P. Frizzo, M. A. P. Martins, M. R. B. Marzari, P. T. Campos, R. M. Claramunt, M. Ángeles García, D. Sanz, I. Alkorta and J. Elguero, *J. Heterocycl. Chem.*, 2010, **47**, 1259–1268.
79 P. Cabildo, R. M. Claramunt, C. López, M. Ángeles García, M. Pérez-Torralba, E. Pinilla, M. Rosario Torres, I. Alkorta and J. Elguero, *J. Mol. Struct.*, 2011, **985**, 75–81.
80 R. Gobetto, C. Nervi, E. Valfre, M. R. Chierotti, D. Braga, L. Maini, F. Grepioni, R. K. Harris and P. Y. Ghi, *Chem. Mater.*, 2005, **17**, 1457–1466.
81 R. Pettinari, F. Marchetti, C. Pettinari, F. Condello, B. W. Skelton, A. H. White, M. R. Chierotti and R. Gobetto, *Dalton Trans.*, 2016, **45**, 3974–3982.
82 F. Marchetti, J. Palmucci, C. Pettinari, R. Pettinari, F. Condello, S. Ferraro, M. Marangoni, A. Crispini, S. Scuri, I. Grappasonni, M. Cocchioni, M. Nabissi, M. R. Chierotti and R. Gobetto, *Chem. – Eur. J.*, 2015, **21**, 836–850.
83 R. Pettinari, C. Pettinari, F. Marchetti, R. Gobetto, C. Nervi, M. R. Chierotti, E. J. Chan, B. W. Skelton and A. H. White, *Inorg. Chem.*, 2010, **49**, 11205–11215.
84 F. Marchetti, C. Pettinari, R. Pettinari, A. Cingolani, R. Gobetto, M. R. Chierotti, A. Drozdov and S. I. Troyanov, *Inorg. Chem.*, 2006, **45**, 3074–3085.
85 J. Viger-Gravel, J. E. Meyer, I. Korobkov and D. L. Bryce, *CrystEngComm*, 2014, **16**, 7285–7297.
86 C. B. Aakeröy, M. Baldrighi, J. Desper, P. Metrangolo and G. Resnati, *Chem. – Eur. J.*, 2013, **19**, 16240–16247.
87 M. Pérez-Torralba, M. Ángeles García, C. López, M. Carmen Torralba, M. Rosario Torres, R. M. Claramunt and J. Elguero, *Cryst. Growth Des.*, 2014, **14**, 3499–3509.
88 Y. Xu, J. Viger-Gravel, I. Korobkov and D. L. Bryce, *J. Phys. Chem. C*, 2015, **119**, 27104–27117.
89 L. Catalano, S. Pérez-Estrada, G. Terraneo, T. Pilati, G. Resnati, P. Metrangolo and M. A. Garcia-Garibay, *J. Am. Chem. Soc.*, 2015, **137**, 15386–15389.
90 M. Weingarth, N. Raouafi, B. Jouvelet, L. Duma, G. Bodenhausen, K. Boujlel, B. Schöllhorn and P. Tekely, *Chem. Commun.*, 2008, 5981–5983.
91 S. P. Brown, M. Pérez-Torralba, D. Sanz, R. M. Claramunt and L. Emsley, *J. Am. Chem. Soc.*, 2002, **124**, 1152–1153.
92 T. N. Pham, S. Masiero, G. Gottarello and S. P. Brown, *J. Am. Chem. Soc.*, 2005, **127**, 16018–16019.
93 S. E. Ashbrook and D. McKay, *Chem. Commun.*, 2016, **52**, 7186–7204.
94 P. M. J. Szell and D. L. Bryce, *Annu. Rep. NMR Spectrosc.*, 2015, **84**, 115–162.
95 P. M. J. Szell and D. L. Bryce, *J. Phys. Chem. C*, 2016, **120**, 11121–11130.
96 R. J. Attrell, C. M. Widdifield, I. Korobkov and D. L. Bryce, *Cryst. Growth Des.*, 2012, **12**, 1641–1653.
97 T. Charpentier, *Solid State Nucl. Magn. Reson.*, 2011, **40**, 1–20.
98 C. Bonhomme, C. Gervais, F. Babonneau, C. Coelho, F. Pourpoint, T. Azais, S. E. Ashbrook, J. M. Griffin, J. R. Yates, F. Mauri and C. J. Pickard, *Chem. Rev.*, 2012, **112**, 5733–5779.
99 J. R. Yates, C. J. Pickard, M. C. Payne and F. Mauri, *J. Chem. Phys.*, 2003, **118**, 5746–5753.
100 F. Alkan, S. T. Holmes, R. J. Iuliucci, K. T. Mueller and C. Dybowski, *Phys. Chem. Chem. Phys.*, 2016, **18**, 18914–18922.
101 G. S. Harbison, in *Characterization of Materials*, John Wiley & Sons, Inc., 2012, pp. 1214–1232.
102 R. Ramachandran and E. Oldfield, *J. Chem. Phys.*, 1984, **80**, 674–677.
103 G. S. Harbison, A. Slokenbergs and T. M. Barbara, *J. Chem. Phys.*, 1989, **90**, 5292–5298.
104 G. K. Semin, T. A. Babushkina, S. P. Khrlakyan, E. Y. Pervova, V. V. Shokina and I. L. Knunyants, *Theor. Exp. Chem.*, **4**, 179–181.
105 G. Bowmaker and S. Hacobian, *Aust. J. Chem.*, 1968, **21**, 551–564.
106 G. Bowmaker and S. Hacobian, *Aust. J. Chem.*, 1969, **22**, 2047–2059.
107 G. A. Bowmaker, *J. Chem. Soc., Faraday Trans. 2*, 1976, **72**, 1964–1969.
108 S. L. Chaplot, G. J. McIntyre, A. Mierzejewski and G. S. Pawley, *Acta Crystallogr., Sect. B: Struct. Crystallogr. Cryst. Chem.* 1981, **37**, 2210–2214.